Chapter 19
Microscopic Simulation of Quantum Cascade Laser Structures

T. Schmielau, M. F. Pereira

Abstract This paper complements recent results on the Nonequilibrium Green's Functions simulations of Quantum Cascade Lasers. Highlights of the main equations are presented here and numerical results for the nonequilibrium density of states are delivered to further illustrate the method, which has reproduced transport experiments in Quantum Cascade Laser structures with very good accuracy.

19.1 Introduction

The systematic exploitation of THz waves has been hindered by the lack of a compact coherent source providing high output power. There is a huge potential for THz technology in a varied list of applications; detecting tumours and skin cancers, pharmaceutical applications, detecting and discriminating explosive threat materials, environmental sensing and gas monitoring, industrial process control, astronomy, semiconductor imaging, security and medical imaging and telecommunications [1, 2]. A number of different materials and systems have been proposed to create compact sources but so far QCLs remain the best candidates for this role [3]. An average THz QCL contains about 1000 layers and takes about eight hours to grow, as compared to the two hours required for a moderately complex commercial device such as a GaAs high electron mobility transistor. Each design has to be optimised for the wavelength chosen, materials used, and growth technique employed, and trade-offs have to be made for pulsed or continuous use, and operating temperature. In fact, it is questionable how often this ideal is actually reached as design and growth are so difficult. The main difficulty so far is to achieve population inversion and it may well be that room temperature operation will only be reached through innovative concepts, like lasing without inversion [4–6]. A fully predictive

T. Schmielau, M. F. Pereira
Materials and Engineering Research Institute, Sheffield Hallam University,
S1 1WB, Sheffield, United Kingdom, e-mail: M.Pereira@shu.ac.uk

M.F. Pereira and O. Shulika (eds.), *Terahertz and Mid Infrared Radiation*: *Generation, Detection and Applications*, NATO Science for Peace and Security Series B: Physics and Biophysics, DOI 10.1007/978-94-007-0769-6_19,

and user-friendly QCL simulator is needed by manufacturers and research teams to design and simulate new devices easily and solve the current technical problems faster. In this paper we complement the material published recently [7–9] on our predictive transport simulator by presenting numerical results for the energetically and spatially resolved electronic density and density of states in a THz QCL.

19.2 Electronic States and Green's Functions Matrix Elements

Electronic states in the QCL are described by in-plane waves with wavevector $\mathbf{k} = (k_x, k_y)$ and (Wannier or position) states $\alpha, \beta \ldots$ in growth direction (z). We put $\alpha = (\mu, m, s)$ and $\beta = (\nu, n, s')$ where m, n indicate the basic period where the state is located and the subband indices μ, ν number the states inside that period. The spin indices $s, s' = \pm 1/2$ are dropped from now on as all occupations and interactions are spin independent. As translational invariance is broken in growth direction, the usual Dyson equation for the retarded GF becomes a matrix equation in the states α, β

$$G^{\mathrm{ret}}_{\alpha\beta,\mathbf{k}}(E) = \left((G^{\mathrm{ret}}_0)^{-1}_{\mathbf{k}}(E) - \Sigma^{\mathrm{ret}}_{\mathbf{k}}(E)\right)^{-1}_{\alpha\beta}, \tag{19.1}$$

where the inverse unperturbed retarded Green's function $(G^{\mathrm{ret}}_0)^{-1}_{\alpha\beta,\mathbf{k}}(E) = E\,\delta_{\alpha\beta} - H^{(0)}_{\alpha\beta} + i\varepsilon$ is determined by the single-particle Hamiltonian $H^{(0)} = H_{\mathrm{kin}} + V_{\mathrm{SL}} + V_{\mathrm{H}} + V_{\mathrm{field}}$ containing kinetic energy, superlattice potential, mean field, and electric potential $V_{\mathrm{field}} = e\mathscr{E}z$ due to the applied electric field $\mathscr{E}$, respectively. In order to reduce the matrix equation to finite size, the periodicity of the superlattice is exploited

$$G_{\mu\, m+n', \nu\, n+n', \mathbf{k}}(E) = G_{\mu m, \nu n, \mathbf{k}}(E + e\mathscr{E}n'd), \tag{19.2}$$

and Green's functions spanning more than two basic periods are assumed to vanish

$$G_{\mu m, \nu n, \mathbf{k}}(E) = 0 \text{ for } |m-n| > 1 \tag{19.3}$$

(sometimes, GFs between more neighbouring periods are kept to check this approximation).

The greater and less components of the GF, which determine the actual occupation of the electronic states, are then obtained from the Keldysh relation

$$G^{>}_{\alpha\beta,\mathbf{k}}(E) = \sum_{\alpha'\beta'} G^{\mathrm{ret}}_{\alpha\alpha',\mathbf{k}}(E) \cdot \Sigma^{>}_{\alpha'\beta',\mathbf{k}}(E) \cdot \left(G^{\mathrm{ret}}_{\beta\beta',-\mathbf{k}}(E)\right)^{*}. \tag{19.4}$$

The additional initial condition term has been omitted from Eq. 19.4 as it vanishes due to dissipation. As a numerical cross-check it has been verified that the Kubo-Martin-Schwinger condition between $G^{>}$ and $G^{<}$ is fulfilled at zero applied voltage, indicating relaxation to thermal equilibrium.

The full Hamiltonian of the system under consideration

$$\hat{H} = \hat{H}_{\mathrm{el}} + \hat{H}_{\mathrm{int}} \tag{19.5}$$

consists of the single particle electron Hamiltonian

$$\hat{H}_{\mathrm{el}} = \sum_{s=\pm 1/2} \int d^3\mathbf{r}\, \hat{a}^{\dagger}(\mathbf{r},s,t)\, H_{\mathrm{el}}(\mathbf{r})\, \hat{a}(\mathbf{r},s,t) \tag{19.6}$$

where $\hat{a}^{\dagger}(\mathbf{r},s,t)$ creates a (conduction band) electron at $\mathbf{r} = (x,y,z)$ and time t with spin s, and the interaction Hamiltonian

$$\hat{H}_{\mathrm{int}} = \hat{H}_{\mathrm{e-e}} + \hat{H}_{\mathrm{e-ion}} + \hat{H}_{\mathrm{LO}} + \hat{H}_{\mathrm{imp}} \tag{19.7}$$

which (in the current state of the simulator) includes electron-electron, electron-LO phonon, and electron-impurity scattering. As band structure and electron-phonon interaction are already accounted for, $\hat{H}_{\mathrm{e-ion}}$ only contains the interaction of the electrons with a homogeneous background charge. Later, first order e-e and e-imp interactions will be combined with this term, superlattice and external potential to form the mean field.

19.3 Numerical Results – Nonequilibrium Density of States

The theory based on the previous equations has reproduced transport data, specially voltage-current curves of THz QCLs with very good accuracy [7]. The Green's Functions inherently carry a wealth of information regarding the electronic system responsible for lasing and by analysing microscopic data and how it influences quantities like the nonequilibrium electronic density and the density of states we can determine how a change in the design can ultimately influence the device performance since all laser related observables like the current, optical gain, refractive index changes etc... will depend on these quantities.

The nonequilibrium electronic density of states (DOS), resolved in both energy and space $\rho(z,E)$ and the electronic density $n_e(z,E)$ are obtained from the correlation Green's Functions components $G^{<}$ by means of the relations

$$\rho(z,E) = -\frac{1}{i\pi A} \sum_{\mathbf{k}\alpha\beta} \Psi^{*}_{\alpha}(z)\, \Psi_{\beta}(z) \left[G^{>}_{\alpha\beta,\mathbf{k}}(E) - G^{<}_{\alpha\beta,\mathbf{k}}(E) \right], \tag{19.8}$$

$$n_e(z,E) = \frac{1}{i\pi A} \sum_{\mathbf{k}\alpha\beta} \Psi^{*}_{\alpha}(z)\, \Psi_{\beta}(z)\, G^{<}_{\alpha\beta,\mathbf{k}}(E),$$

where A is the sample area. They are depicted in Fig. 19.1. The DOS is the number of states at each energy level that are available to be occupied. Here we sum over states so we cannot target specific levels, but can look at pockets of states. There is

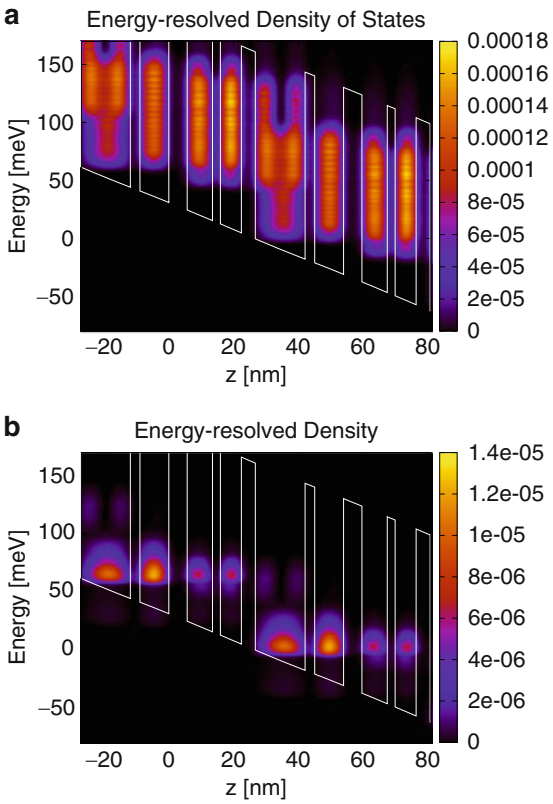

Fig. 19.1 Energy and frequency resolved density of states (a) and electronic density (b) after Eq. 19.9 for the QCL structure of Ref. [11]

a large density of states in the active region of the device ($5.5\,\text{nm} < z < 22.4\,\text{nm}$). The density plots shows regions with high occupation around the upper lasing levels. Each of these plots together with other quantities, like the actual population inversion, transition dipole moments, frequency and momentum dependent dephasing and spectral functions [8, 9] lead to further microscopic insight into the system and altogether can help to understand the microscopic reason for operation bottlenecks. Similar plots have already helped to understand the operation of mid infrared quantum cascade laser [10] and here we go a step beyond show results with full frequency and momentum dependent selfenergies including dynamically screened electron-electron scattering [7] for a THz device.

In summary our efficient Nonequilibrium Green's Functions simulations can provide microscopic insight about new materials and devices and can be used to create and optimise new devices. It can become a valuable tool in the development of THz quantum cascade lasers operating at high temperature.

References

[1] M.E. Portnoi, O.V. Kibis, M. Rosenau da Costa, Superlattices and Microstructures 43, 399 (2008).
[2] M.F. Pereira, Journal of Telecommunications and Information Technology 4, 118 (2009).
[3] R. Kohler, A. Tredicucci, F.Beltram, H.E.Beere, E.H.Linfield, G.A.Davies and D.A.Ritchie, Advances in Solid State Physics 43, 327 (2003).
[4] A. Wacker, Nat. Phys. 3, 298 (2007).
[5] R. Terazzi, T. Gresch, M. Giovanni, N. Hoyler, F. Faist, and N. Sekine, Nat. Phys. 3, 329 (2007).
[6] M. F. Pereira Jr., Phys. Rev. B, vol. 78, 245305-1 (2008).
[7] T. Schmielau and M.F. Pereira, Appl. Phys. Lett. 95, 231111 (2009).
[8] T. Schmielau and M.F. Pereira, Microelectronics Journal 40, 869 (2009).
[9] T. Schmielau and M.F. Pereira, physica status solidi b 246, 329 (2009).
[10] R. Nelander, A. Wacker, M.F. Pereira Jr., D.G. Revin, M.R.Soulby, L.R. Wilson, J.W. Cockburn, A.B. Krysa, J.S. Roberts, and R.J. Airey, Journal of Applied Physics 102, 113104 (2007).
[11] S. Kumar, B. S. Williams, S. Kohen, Q. Hu and J. Reno, Appl. Phys. Lett. 84, 2494 (2004).